Supporting Information

Directionally Guided Droplets on a Modular Bottom-Up Anisotropic Locally Ordered Nickel Nanocone Superhydrophobic Surface

Ruiqing Zou, [1] *Jian Wang,* [*,1] *Jianbin Tang,* [1] *Xin Zhang,* [1] *Yaocheng Zhang*[*,2]

[1] School of Materials Science and Enginering, Xihua University, Chengdu 610039, People's Republic of China

[2] School of Automotive Engineering, Changshu Institute of Technology, Jiangsu 215500, People's Republic of China

*Corresponding author.

E-mail address: wangjianxhu@163.com (Jian Wang)

Postal address: No. 999 Jinzhou Road, Chengdu 610039, People's Republic of China

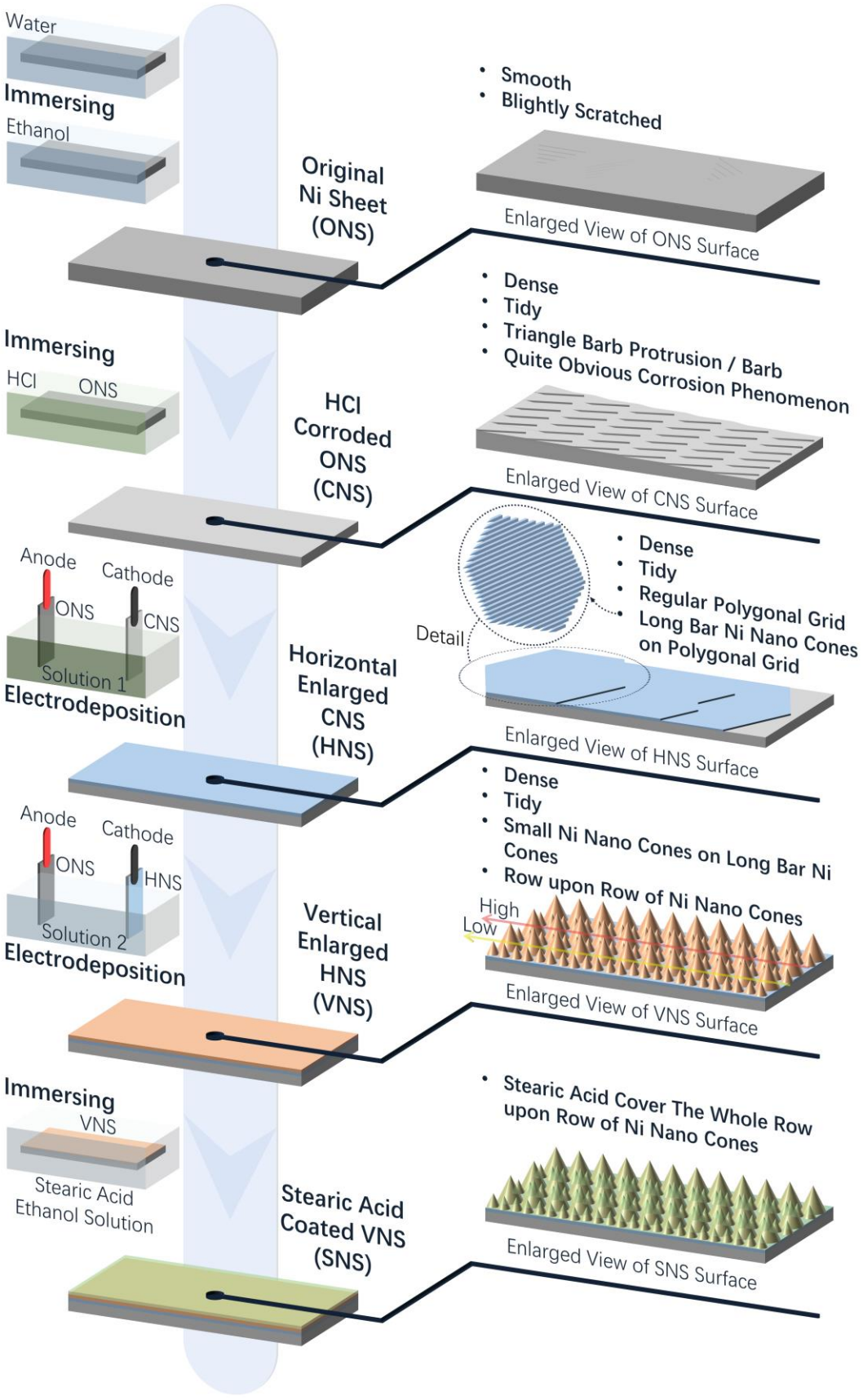

Figure S1. The preparation procedure, each stage state and possible

morphology of superhydrophobic SNS.

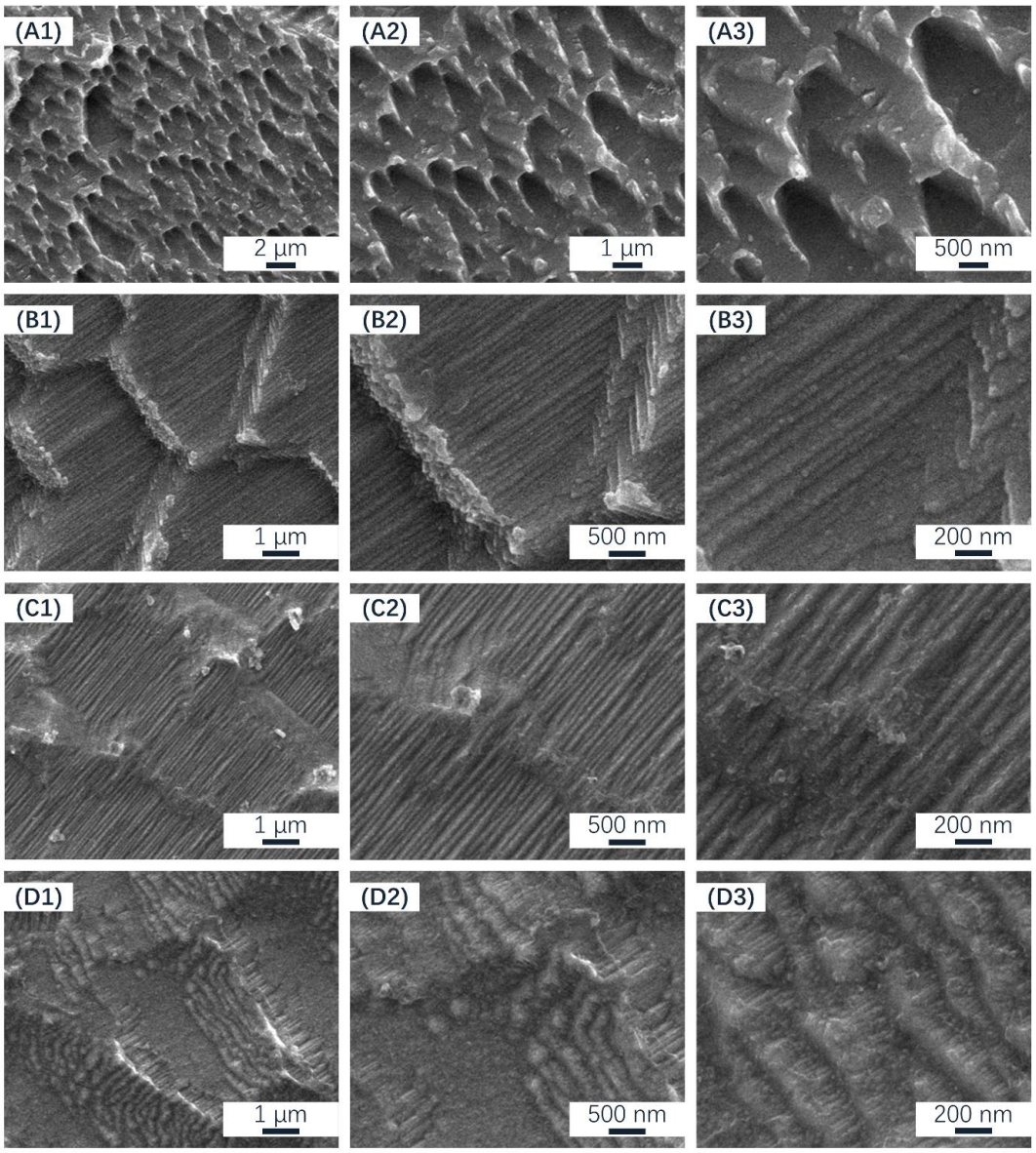

Figure S2. The low and high magnification SEM images of CNS (A1-A3), HNS-10 (B1-B3), HNS-15 (C1-C3) and HNS-20 (D1-D3). The Ni sheet corroded by HCl are covered with dense spikes (A1), stacked on top of each other (A2) and similar in size (A3). HNS-10 has obvious polygonal grids (B1), where grooves arranged tightly and neatly (B2), and the tip of each groove is similar to the spikes on CNS (B3). The polygonal grids are slightly blurred on HNS-15 (C1), where grooves become more

visible and deeper (C2), and spikes at the tip of groove disappeared (C3). The stacking of grids on HNS-20 has become more and more serious (D1), where the space of grooves is almost squeezed out (D2), and the tip of groove is difficult to observe (D3).

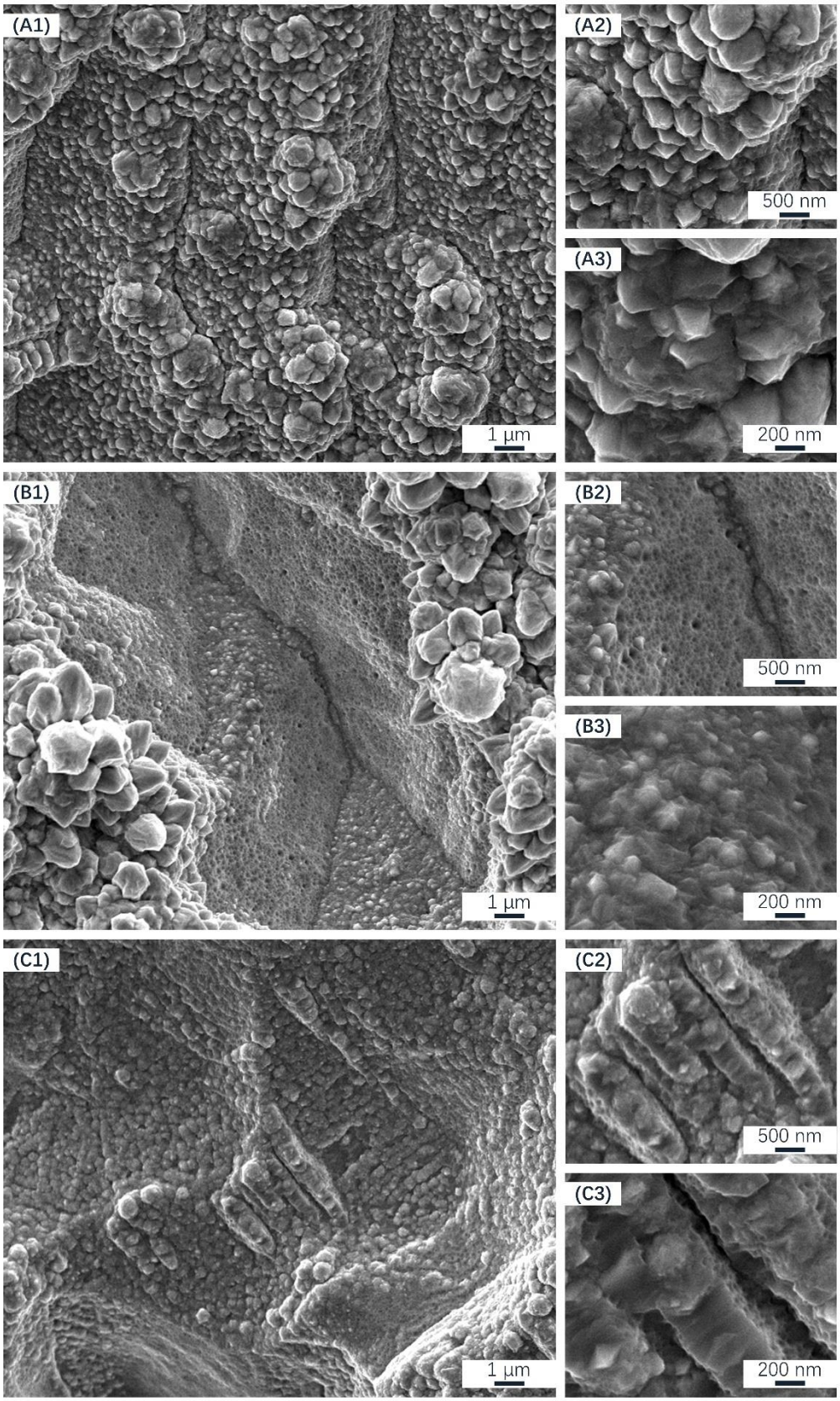

Figure S3. The low and high magnification SEM images of VNS-10 (A1-

A3), VNS-15 (B1-B3) and VNS-20 (C1-C3). The surface of VNS-10 is composed of dense and regularly arranged Ni nano cones, where although the “gullies” is shallow, they effectively distinguish the different “mountains” (A1), while on the “peaks”, the Ni nano cones (A2), where some layered texture could be vaguely discerned (A3), show a horizontal growth trend. The surface of VNS-15 is composed of extremely deep “gullies” and extremely high “mountains”, where exist dense Ni nano cones, which grow like flowers blooming (B1), while the “gullies” consist of a large number of holes and Ni nano cones (B2), which are too small to be got deserved concern, but just be considered as ungrown Ni nano cones (B3). The surface of VNS-20 is composed of locally artfully arranged sheet-like structures (C1), which are stacked together and mainly composed of Ni nano cones and holes (C2) that seem to penetrate the entire sheet-like structure (C3).

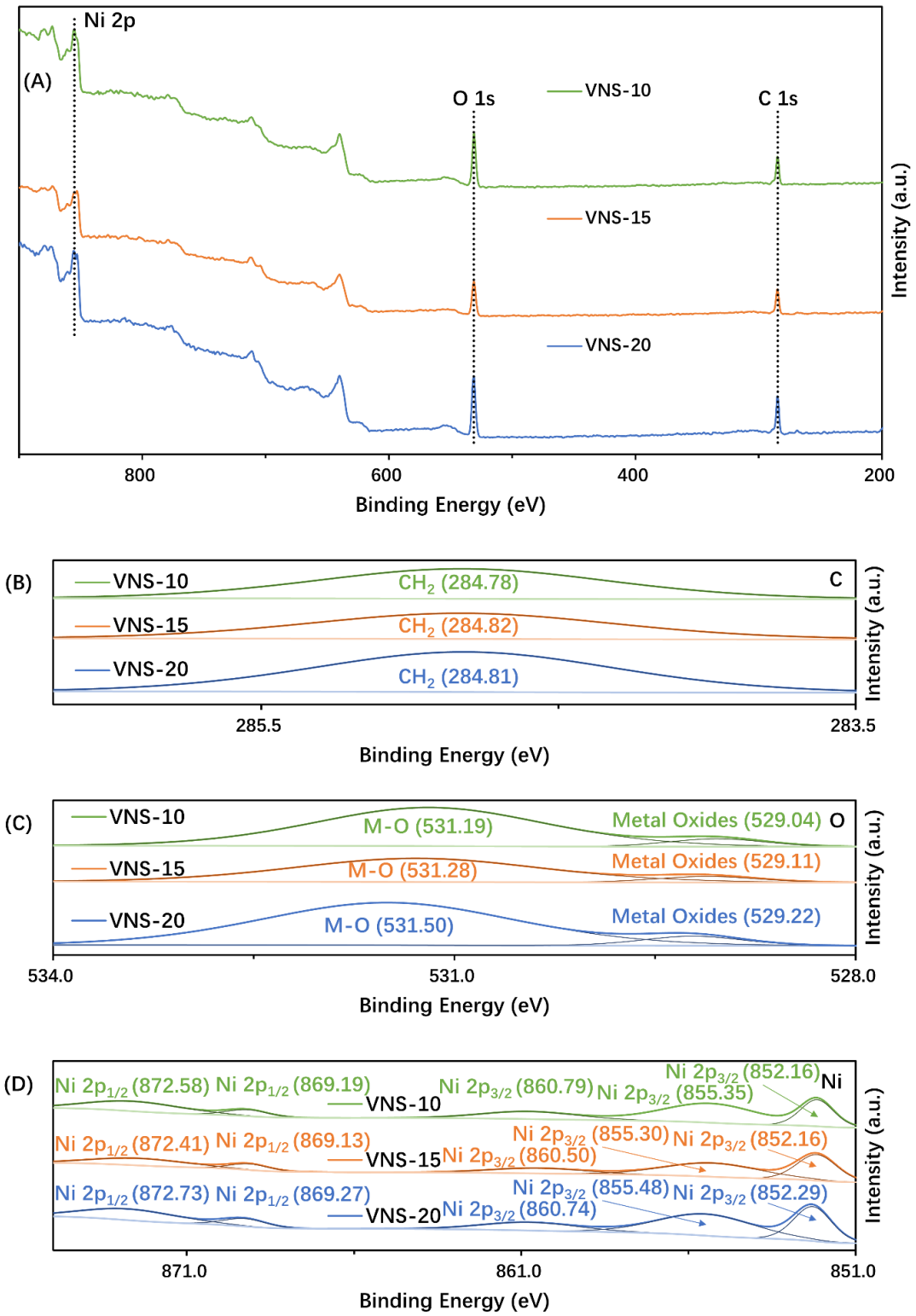

Figure S4. (A) is the XPS full survey spectra of VNSs, where the peaks of C 1s, O 1s and Ni 2p have been detected. The VNSs C 1s HR-XPS spectrum is shown in (B), where could be only recognized one peak, which could be identified as $-CH_2$ due to the dust, each sample at 284.78

eV (VNS-10, green line), 284.82 eV (VNS-15, orange line) and 284.81 eV (VNS-20, blue line), respectively. The VNSs O 1s HR-XPS spectrum is shown in (C), where could be divided into 2 different peaks, which could be attributed to M-O and Metal Oxides due to the natural oxidation of metallic Ni in the air, each sample at 531.19 and 529.04 eV (VNS-10, green line), 531.28 and 529.11 eV (VNS-15, orange line), 531.50 and 529.22 eV (VNS-20, blue line), respectively. The VNSs Ni 2p HR-XPS spectrum is shown in (D), where could be divided into 5 different peaks, which could be attributed to Ni $2p_{1/2}$ and Ni $2p_{3/2}$ with a significantly split spin-orbit components (Δ_{metal} = 17.23 (VNS-10, green line), 17.11 (VNS-15, orange line) and 17.25 (VNS-20, blue line) eV), which indicated that Ni element exists on the surface of VNSs in the form of Ni^{2+}, each sample at 872.58, 869.19 eV (Ni $2p_{1/2}$, VNS-10, green line) and 860.79, 855.35, 852.16 eV (Ni $2p_{3/2}$, VNS-10, green line); 872.41, 869.13 eV (Ni $2p_{1/2}$, VNS-15, orange line) and 860.50, 855.30, 852.16 eV (Ni $2p_{3/2}$, VNS-15, blue line); 872.73, 869.27 eV (Ni $2p_{1/2}$, VNS-20, blue line) and 860.74, 855.48, 852.29 eV (Ni $2p_{3/2}$, VNS-20, blue line), respectively.

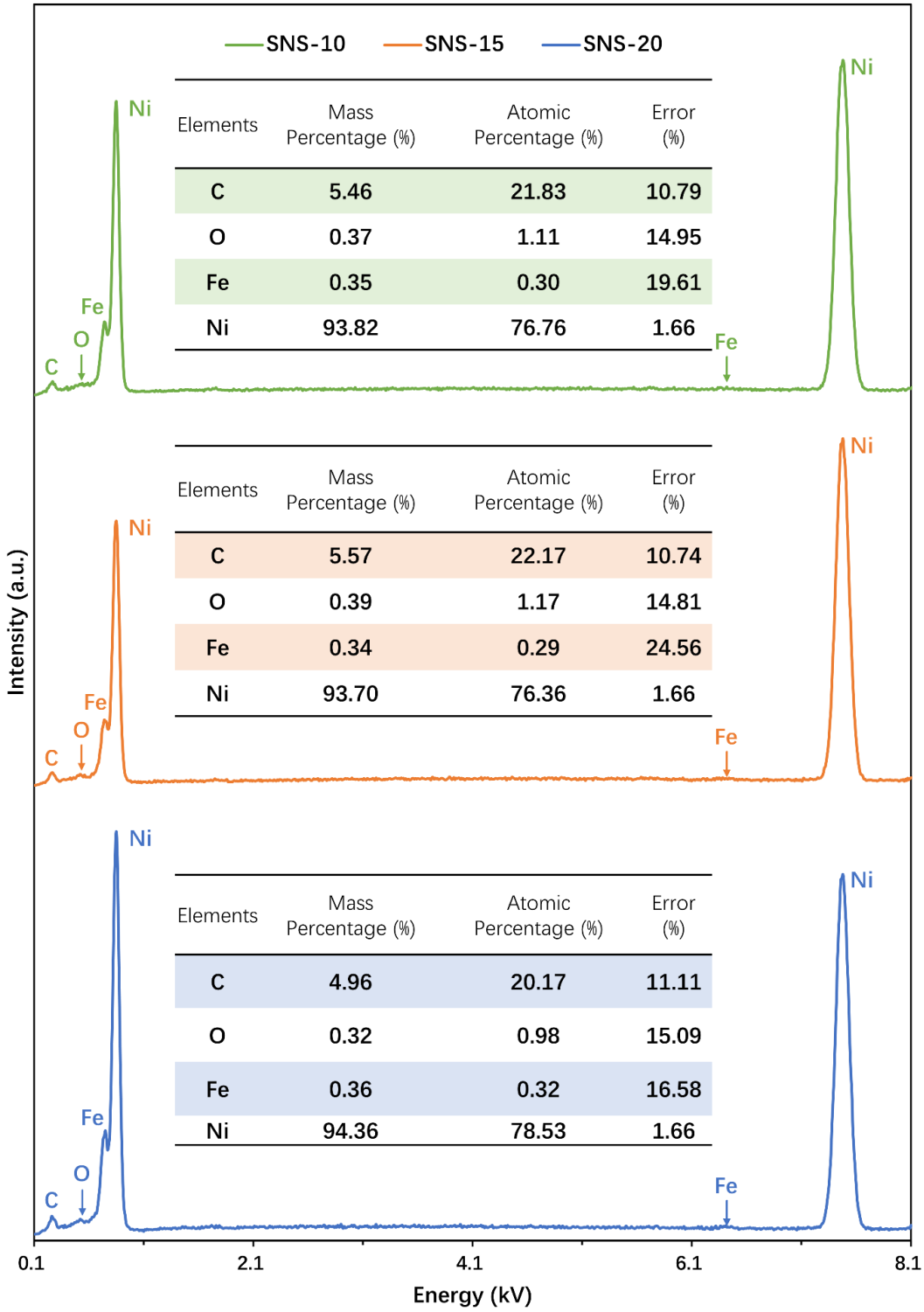

Figure S5. The EDS spectrum of SNSs is composed of Ni, C and O elements and extraordinarily little Fe element, which is due to the residue of horizontal enlarged process and consistent with the reduction-replacement-reduction cycle mechanism discussed above. The phenomena

that Ni element occupies the majority, followed by C element, O element and Fe element, respectively, is applicable to every specific sample (SNS-10, green line; SNS-15, orange line; SNS-20, blue line).

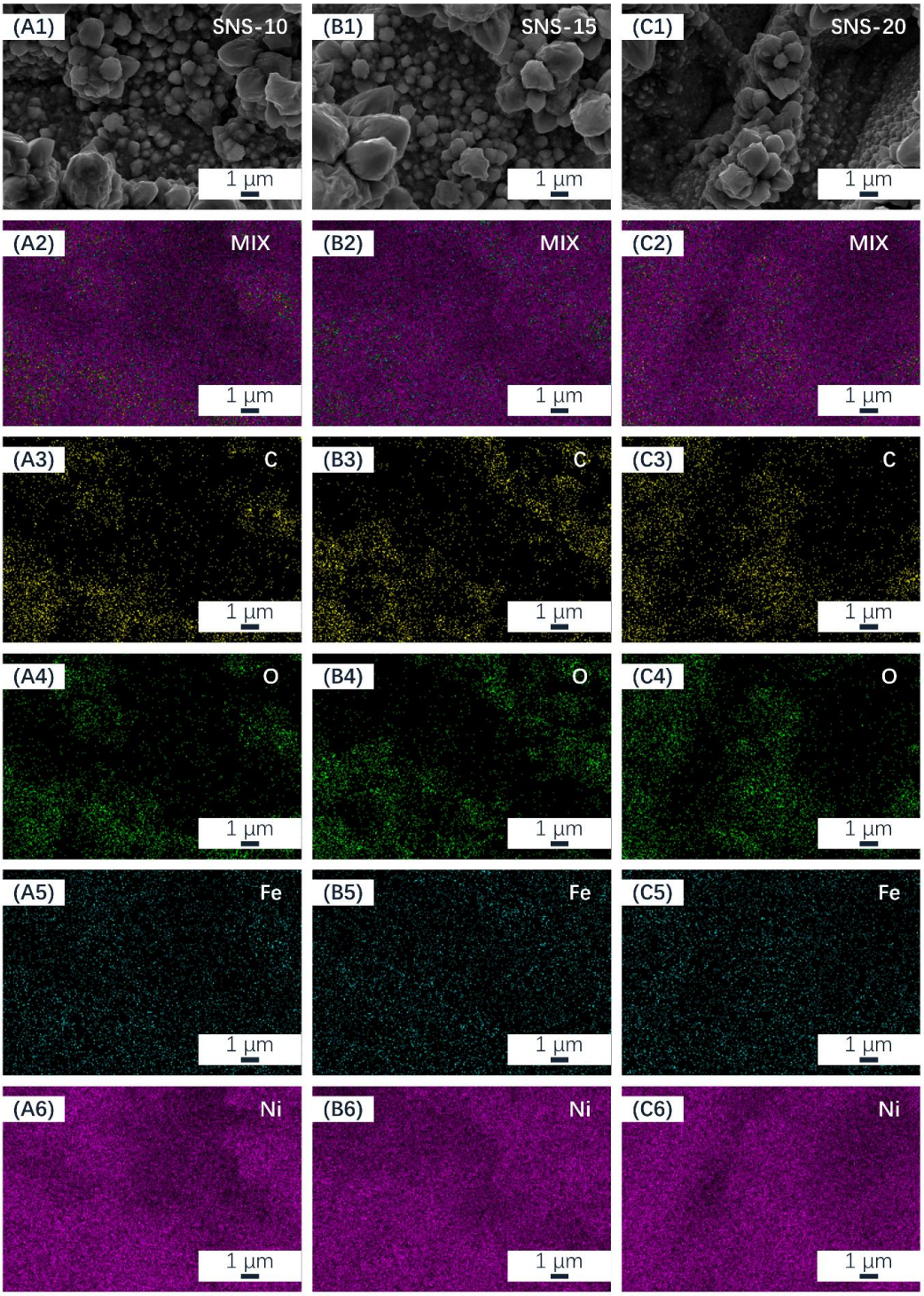

Figure S6. The EDS mapping images of SNSs. The phenomena that the

enrichment areas of element C and O are consistent in the protrusions (A3, A4, B3, B4, C3, C4), the distribution of element Fe is relatively uniform without obvious enrichment (A5, B5, C5), and element Ni, which occupies an absolute high concentration, is enriched everywhere (A6, B6, C6), respectively, is applicable to every specific sample (SNS-10, A1-A6; SNS-15, B1-B6; SNS-20, C1-C6).

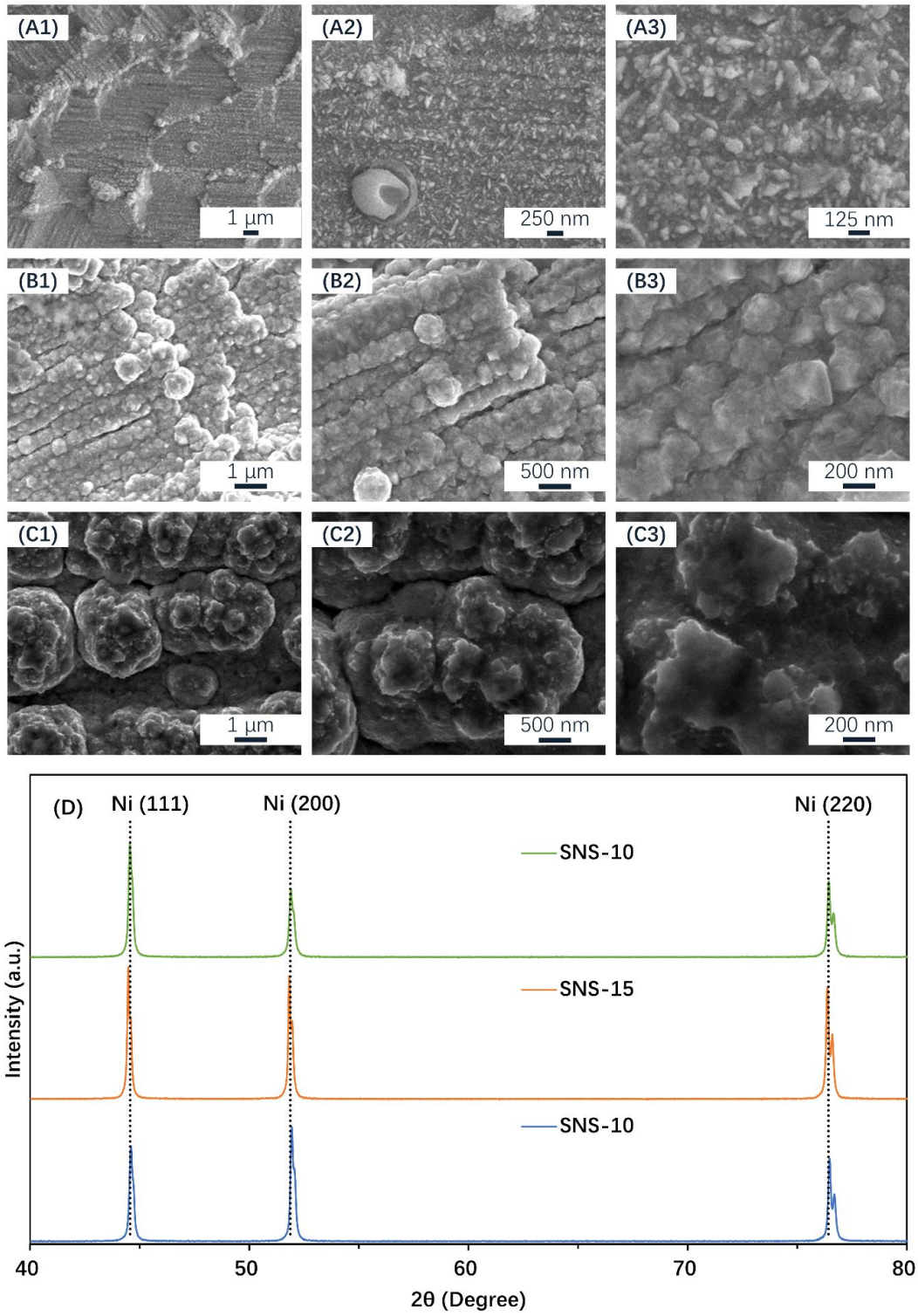

Figure S7. The low and high magnification SEM images of SNS-10 (A1-A3), SNS-15 (B1-B3) and SNS-20 (C1-C3). On the surface of SNS-10, there are still obvious grids and artfully arranged grooves (A1), where have been composed of tiny Ni nano cones (A2), which are spontaneously

arranged along a straight line with obvious shallow gullies between each other (A3). And on the surface of SNS-15, there is an obvious stepped morphology (B1), where exists the neat arrangements of dense Ni nano cones, which are densely connected to each other (B2), and the resulting narrow and deep gullies, which caused the difference of height (B3). While on the surface of SNS-20, huge Ni nano cylinders arranged neatly are connected to each other to form a neat arrangement, where the alignments are far apart to form a wide ravine, and the top of these Ni nano pillars are composed of flat Ni nano flowers. The XRD patterns of SNS-10, SNS-15, and SNS-20 are presented in (D), where only Ni peaks have been detected. Peaks at 44.56°, 51.91° and 76.44° detected on SNS-10 (green line) are assigned to (111), (200) and (220) planes of Ni; peaks at 44.49°, 51.82° and 76.37° detected on SNS-15 (orange line) are assigned to (111), (200) and (220) planes of Ni; peaks at 44.61°, 51.94° and 76.47° detected on SNS-20 (blue line) are assigned to (111), (200) and (220) planes of Ni, respectively, and these whole diffraction peaks of Ni are found to consistent with pure Ni phase having fcc structure, due to the standard card (JCPDS No. 04-0850).

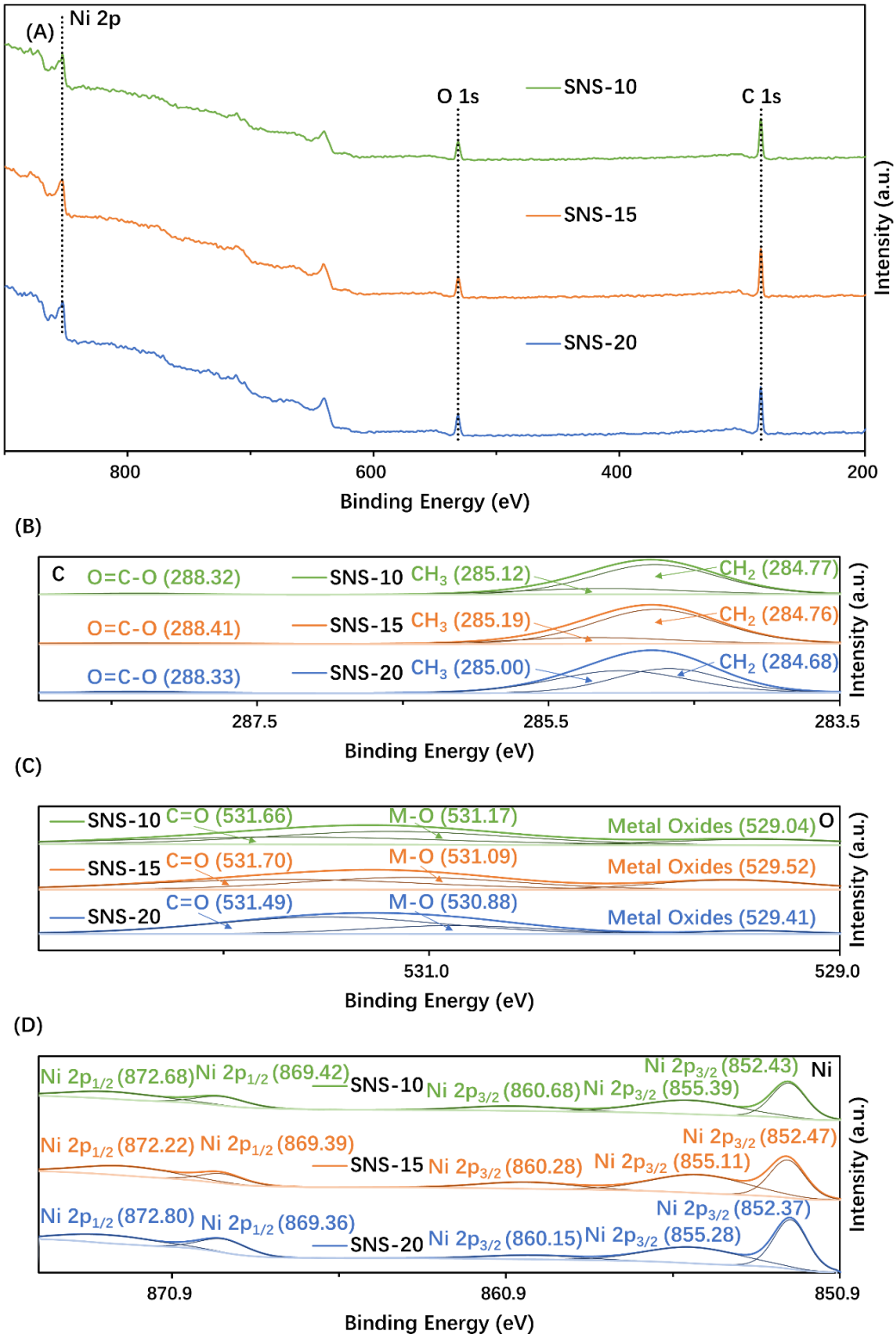

Figure S8. (A) is the XPS full survey spectra of SNSs, where the peaks of C 1s, O 1s and Ni 2p have been detected. The SNSs C 1s HR-XPS spectrum is shown in (B), where could be divided into 3 different peaks,

which could be identified as O=C-O, $-CH_3$ and $-CH_2$ due to the stearic acid, each sample at 288.32, 285.12 and 284.77 eV (SNS-10, green line); 288.41, 285.19 and 284.76 eV (SNS-15, orange line); 288.33, 285.00 and 284.68 eV (SNS-20, blue line), respectively. The SNSs O 1s HR-XPS spectrum is shown in (C), where could be divided into 3 different peaks, too, which could be attributed to C=O, M-O and metal oxides due to the stearic acid, Ni-O bonds and natural oxidation of metallic Ni in the air, each sample at 531.66, 531.17 and 529.04 eV (SNS-10, green line); 531.70, 531.09 and 529.52 eV (SNS-15, orange line); 531.49, 530.88 and 529.41 eV (SNS-20, blue line), respectively. The SNSs Ni 2p HR-XPS spectrum is shown in (D), where could be divided into 5 different peaks, which could be attributed to Ni $2p_{1/2}$ and Ni $2p_{3/2}$ with a significantly split spin-orbit components (Δ_{metal} = 17.29 (SNS-10, green line), 17.11 (SNS-15, orange line) and 17.52 (SNS-20, blue line) eV), which indicated that Ni element exists on the surface of SNSs in the form of Ni^{2+}, each sample at 872.68, 869.42 eV (Ni $2p_{1/2}$, SNS-10, green line) and 860.68, 855.39, 852.43 eV (Ni $2p_{3/2}$, SNS-10, green line); 872.22, 869.39 eV (Ni $2p_{1/2}$, SNS-15, orange line) and 860.28, 855.11, 852.47 eV (Ni $2p_{3/2}$, SNS-15, blue line); 872.80, 869.36 eV (Ni $2p_{1/2}$, SNS-20, blue line) and 860.15, 855.28, 852.37 eV (Ni $2p_{3/2}$, SNS-20, blue line), respectively.

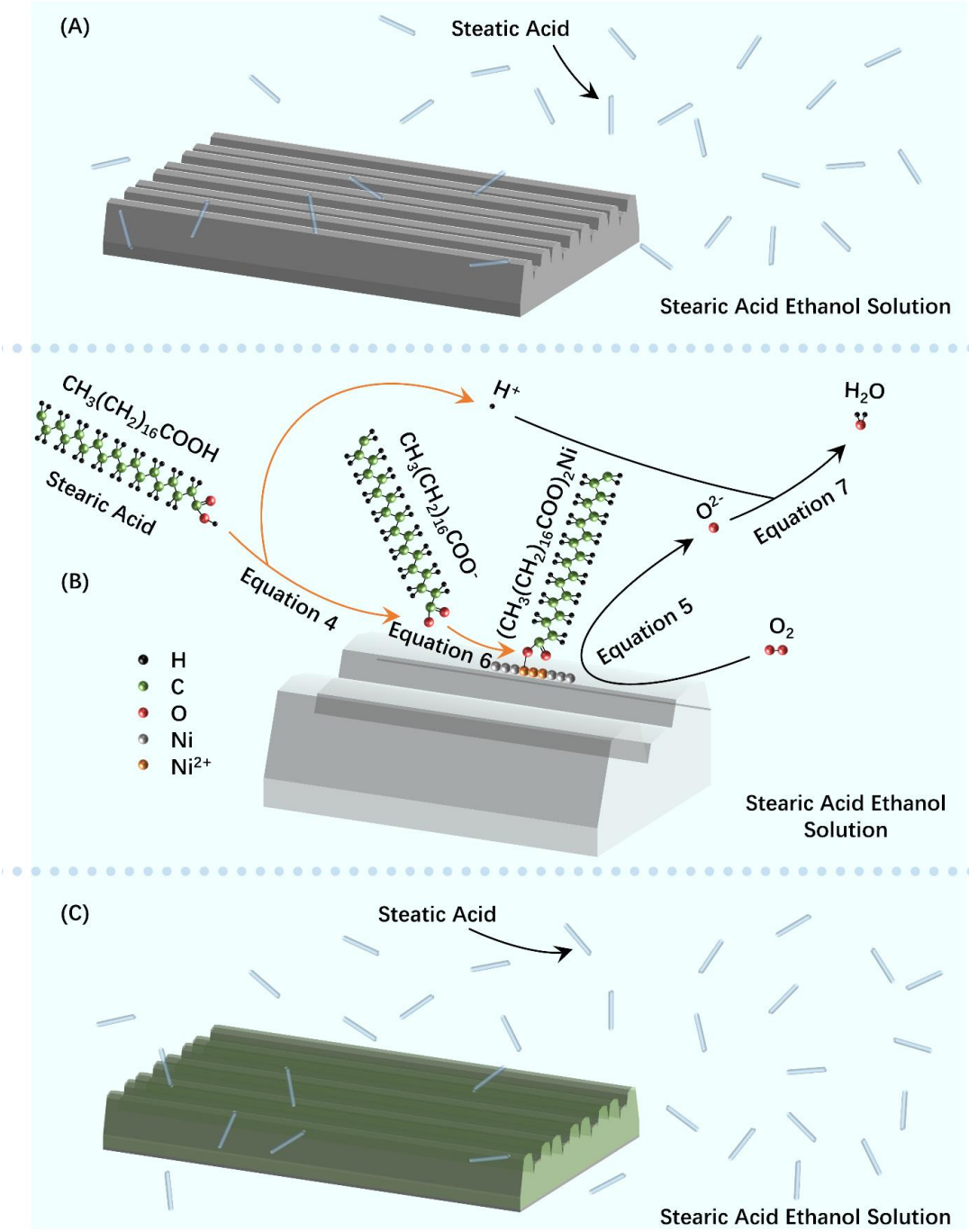

Figure S9. Immerse VNSs in the stearic acid ethanol solution (A). Oxygen, which would be finally reduced to O^{2-}, oxidizes the Ni atoms on the surface of VNSs to Ni^{2+}. At the same time, stearic acid in the solution reacts with Ni^{2+} in the form of stearate ions to form Ni-O bonds ($(CH_3(CH_2)_{16}COO)_2Ni$), and free O^{2-} react with H^+ to produce water (B). Then, gradually, the surface of VNSs would been covered with

stearic acid, forming SNSs (C).

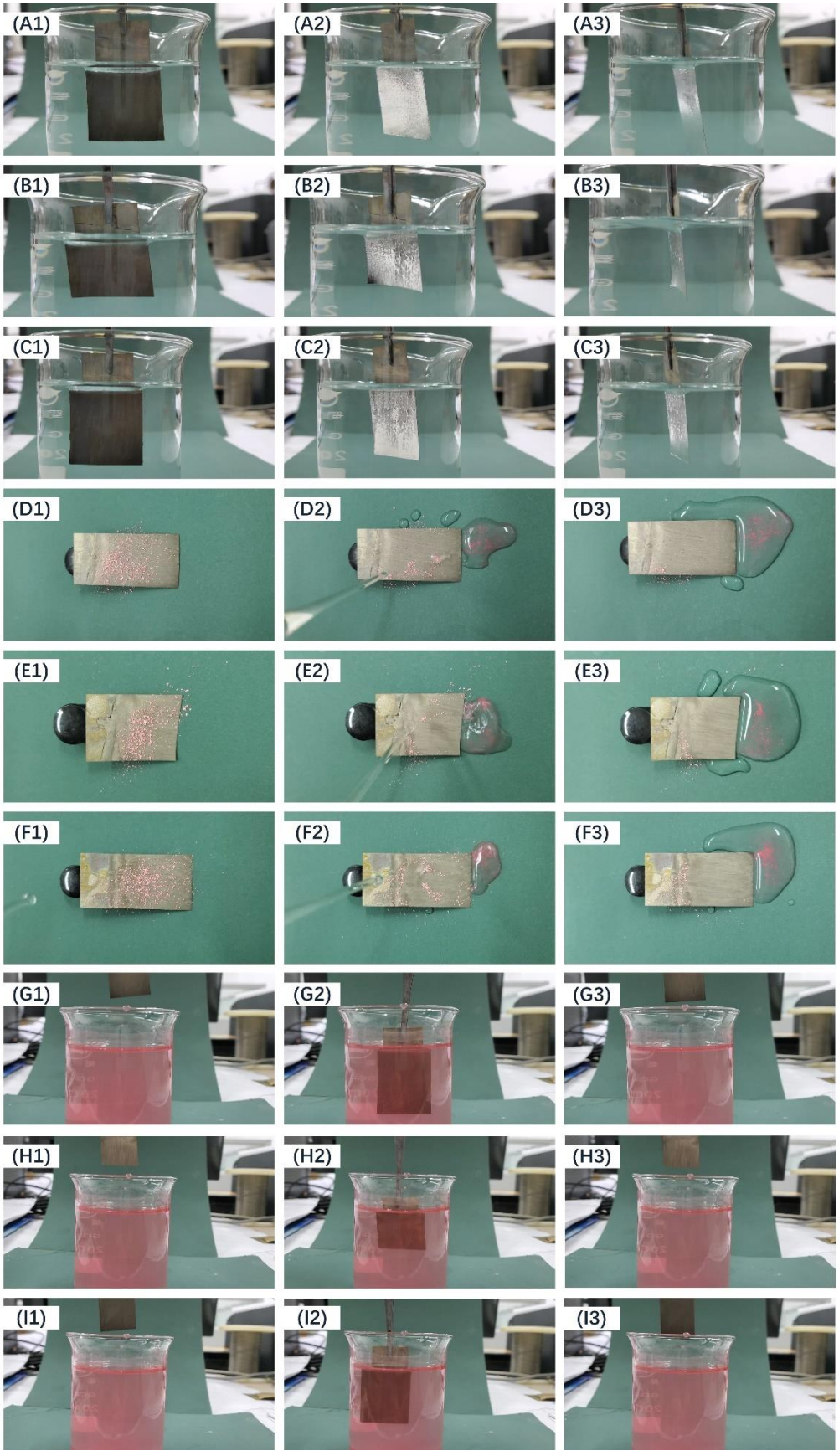

Figure S10. Mirrorlike effect of SNS-10 (A1-A3), SNS-15 (B1-B3), and

SNS-20 (C1-C3) immersed in water at different angles, respectively. The self-cleaning phenomena (b-i) of SNS-10 (D1-D3), SNS-15 (E1-E3), and SNS-20 (F1-F3), which have been covered by pink impurities, respectively. The antifouling phenomena of SNS-10 (G1-G3), SNS-15 (H1-H3), and SNS-20 (I1-I3), which are immersed in water containing insoluble impurities, respectively.

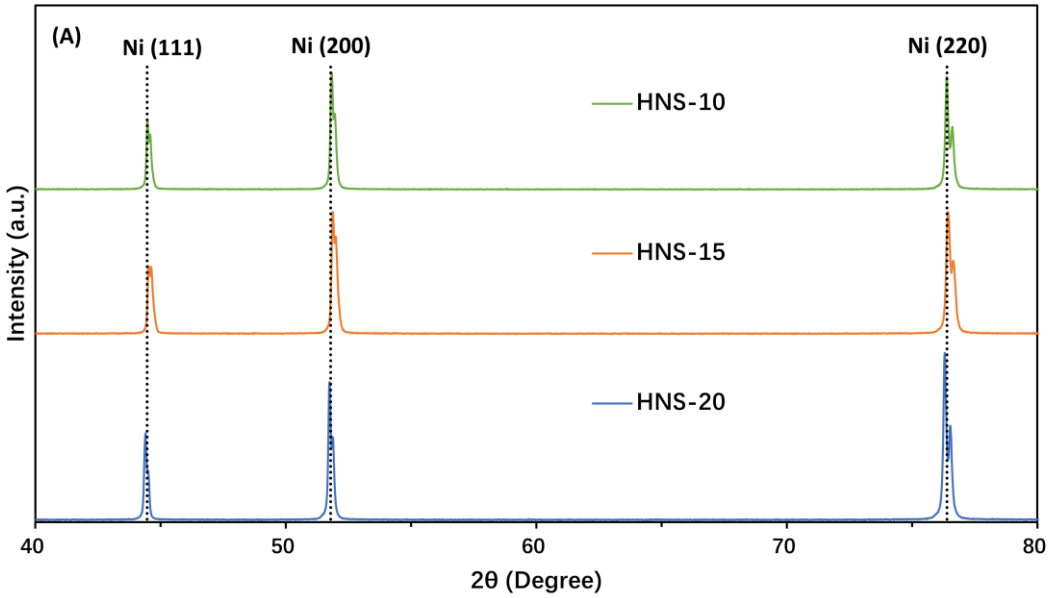
(A)
Ni (111)
Ni (200)
Ni (220)
HNS-10
HNS-15
HNS-20
Intensity (a.u.)
40
50
60
70
80
2θ (Degree)

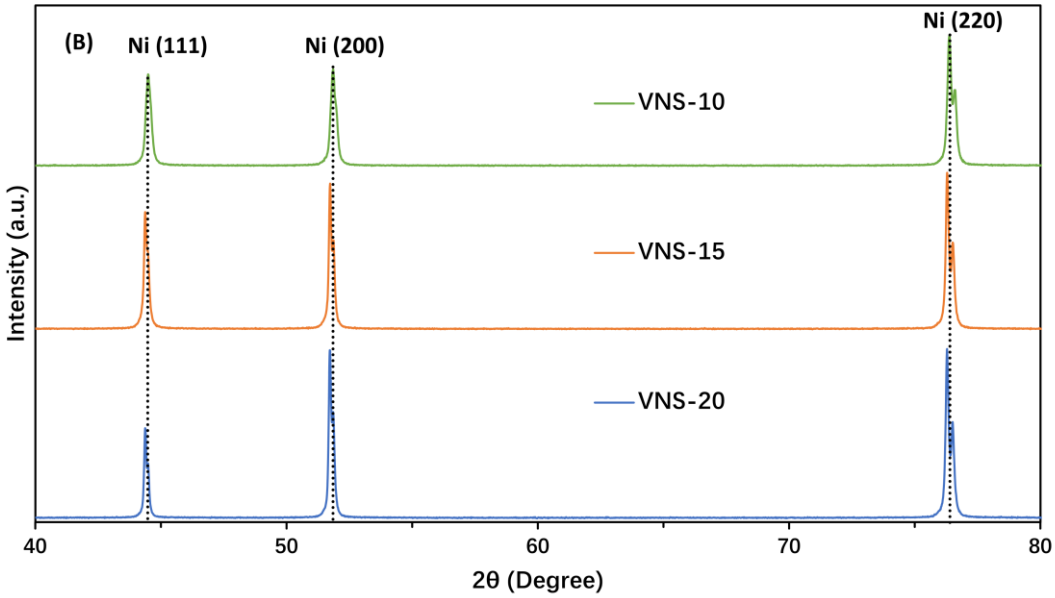
(B)
Ni (111)
Ni (200)
Ni (220)
VNS-10
VNS-15
VNS-20
Intensity (a.u.)
40
50
60
70
80
2θ (Degree)

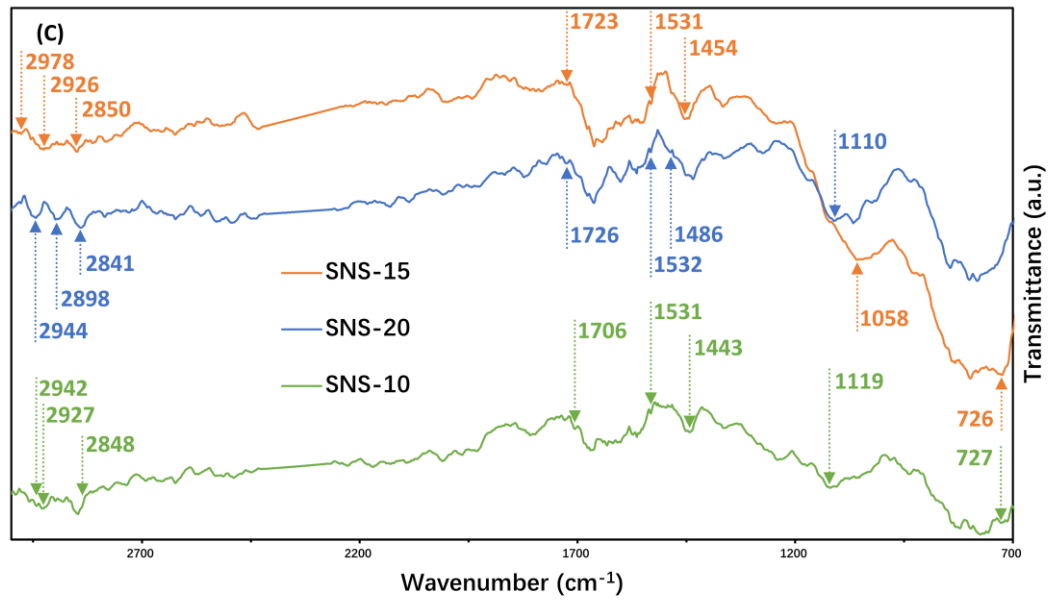
(C)
2978
2926
2850
1723
1531
1454
1110
1726
1486
1532
2841
2898
2944
SNS-15
SNS-20
SNS-10
1058
1706
1531
1443
1119
2942
2927
2848
726
727
Transmittance (a.u.)
2700
2200
1700
1200
700
Wavenumber (cm-1)

Figure S11. The XRD patterns of HNS-10, HNS-15, and HNS-20 are presented in (A); The XRD patterns of VNS-10, VNS-15, and VNS-20 are presented in (B); (C) is the FTIR spectra of SNSs.

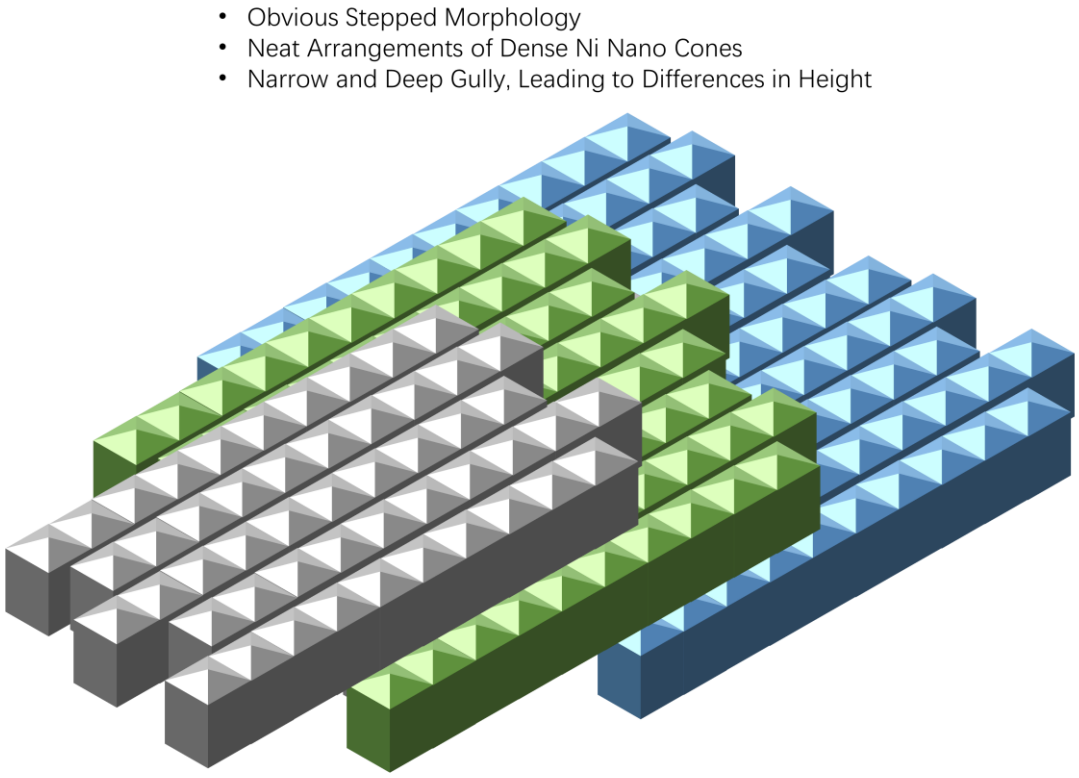

Figure S12. The schematic diagram of the structure of SNS-15.

Table S1. Formulation of electrodeposition solution 1.

Name	Concentration ($mol \cdot L^{-1}$)
$NiCl_2 \cdot 6H_2O$	0.421
H_3BO_3	0.809
NH_4Cl	0.748
$Fe(NO_3)_3 \cdot 9H_2O$	0.364

Table S2. Formulation of electrodeposition solution 2.

Name	Concentration ($mol \cdot L^{-1}$)
H_3BO_3	0.809

NH_4Cl	0.374

Table S3. The naming rules of Ni sheets treated with different electrodeposition time and current density.

Purification	ONS		
HCl Corrosion	Time: 60 min Temperature: 80 ℃ CNS		
Horizontal Enlargement	Time: 10 min Current: 0.1 A HNS-10	Time: 15 min Current: 0.1 A HNS-15	Time: 20 min Current: 0.05 A HNS-20
Vertical Enlargement	Time: 30 min Current: 0.1 A VNS-10	Time: 30 min Current: 0.1 A VNS-15	Time: 30 min Current: 0.1 A VNS-20
Superhydrophobization	Time: 120 min Temperature: 30 ℃ SNS-10	Time: 120 min Temperature: 30 ℃ SNS-15	Time: 120 min Temperature: 30 ℃ SNS-20

Table S4. Some calculation parameters, results, and formulas related to the porosity of SNS-15, where θ_r is the CA of SNS-15 and θ_1 is the CA of stearic acid coated CNS-15, f_1 and f_2 refers to the ratio of the actual contact area of solid-liquid interface to the apparent contact area and refers to the ratio of the actual contact area of gas-solid interface to the apparent contact area, respectively. The sum of f_1 and f_2 is one (Equation S3). Since θ_1 and θ_2 are the intrinsic CA of liquid on solid-liquid and gas-liquid interfaces, respectively, θ_2 =

180°, and Equation (S1) could be rewritten as Equation (S2) and (S4).

	θ_r (°)	θ_1 (°)	f_1 (%)	f_2 (%)
SNS-15	163.200	133.700	13.807	86.193
Equations	$\cos\theta_r = f_1\cos\theta_1 + f_2\cos\theta_2$			(Equation S1)
	$\cos\theta_r = f_1\cos\theta_1 - f_2$			(Equation S2)
	$f_1 + f_2 = 1$			(Equation S3)
	$\cos\theta_r = f_1\cos\theta_1 - 1 + f_1$			(Equation S4)

Table S5. Some calculation parameters, results, and formulas of SNS-15 surface free energy, where γ_S^D is the contribution of the surface free energy dispersion part of the solid surface, γ_S^P is the surface free energy contributed by the solid polar components, and γ_S is the surface free energy of the solid, and similarly, γ_L is the liquid surface free energy, γ_L^D is the liquid dispersion surface free energy, γ_L^P is the surface free energy of the polar components of the liquid, and θ is the CA, calculated via the Owen two-liquid method (water and diiodomethane).

	Surface Tension Parameters of Liquid (mJ m^{-2})		
	γ_L	γ_L^D	γ_L^P
Water	72.800	21.800	51.000
Diiodomethane	50.800	48.500	2.300
	Surface Tension Parameters of Solid (mJ m^{-2})		
	γ_S	γ_S^D	γ_S^P
SNS-15	8.516	6.617	1.899
Equations	$\gamma_S = \gamma_S^D + \gamma_S^P$		(Equation S5)

$$\sqrt{\gamma_S^D \cdot \gamma_L^D} + \sqrt{\gamma_S^P \cdot \gamma_L^P} = \gamma_L \cdot \frac{\cos\theta+1}{2} \quad \text{(Equation S6)}$$

Table S6. Some calculation parameters, results and formulas related to the adhesion work of SNSs and to the solid-liquid interfacial tension of SNS-15. The adhesion work together with Young's Equation and Dupree Equation, which could be represented by Equation (S7) and (S8), where W_a is the adhesion work.

	SNS-10	SNS-15	SNS-20
W_a ($mJ \cdot m^{-2}$)	7.935	3.107	1.173
γ_{S-L} ($mJ \cdot m^{-2}$)	-	78.209	-

Equations

$$W_a = 2\left(\sqrt{\gamma_S^D \cdot \gamma_L^D} + \sqrt{\gamma_S^P \cdot \gamma_L^P}\right) \quad \text{(Equation S7)}$$

$$W_a = \gamma_{L-G}(1 + \cos\theta_r) \quad \text{(Equation S8)}$$

$$\gamma_{S-L} = \gamma_S + \gamma_L - W_a \quad \text{(Equation S9)}$$

$$\gamma_{S-L} = \gamma_S + \gamma_L - 2\left(\sqrt{\gamma_S^D \cdot \gamma_L^D} + \sqrt{\gamma_S^P \cdot \gamma_L^P}\right) \quad \text{(Equation S10)}$$

Video S1. The SA (//) of SNS-10

Video S2. The SA (⊥) of SNS-10

Video S3. The SA (//) of SNS-20

Video S4. The SA (⊥) of SNS-20

Video S5. The SA (//) of SNS-15

Video S6. The SA (⊥) of SNS-15

Video S7. Bounce process on SNS-15

Video S8. Merge process on SNS-15

Video S9. Mirrorlike effect of SNS-10

Video S10. Mirrorlike effect of SNS-15

Video S11. Mirrorlike effect of SNS-20

Video S12. Self-cleaning of SNS-10

Video S13. Self-cleaning of SNS-15

Video S14. Self-cleaning of SNS-20

Video S15. Antifouling of SNS-10

Video S16. Antifouling of SNS-15

Video S17. Antifouling of SNS-20